The Carousel Effect in Alveolar Models

F. E. Laine-Pearson and P. E. Hydon *

Abstract

Background. *Experimental work over the past decade has shown that recirculation in alveoli substantially increases the transport of particles. We have previously shown that, for nondiffusing passive particles, this can be understood with the aid of Moffatt's famous corner flow model. Without wall motion, passive particles recirculate in a regular fashion and no chaos exists; however, wall motion produces extensive chaotic flow. Aerosols typically do not follow this flow, instead they diffuse. Here we construct a simple model to study diffusing particles in the presence of recirculation.*

Method of Approach. *We assume all particles are passive, that is to say they do not alter the underlying flow significantly. We modify the Lagrangian system for corner eddies to accommodate diffusing particles. Particle transport is governed by Langevin equations. Ensembles of diffusing particles are tracked by numerical integration.*

Results. *We show that transport of diffusing particles is enhanced by sufficiently strong underlying recirculation through a mechanism that we call the 'carousel effect'. However, as the corner is approached, the recirculation rapidly decreases in intensity, favouring motion by diffusion. Far from the corner's apex, recirculation dominates.*

Conclusions. *For real alveoli, the model indicates that transport of aerosols is enhanced by sufficiently strong recirculation.*

Keywords: *physiological fluid flows, Lagrangian dynamics, diffusing particles*

1 Background

The purpose of this paper is to explore the effect of recirculation on the transport of diffusing particles in the pulmonary alveolus. Our motivation for this investigation comes from wanting to quantify the movement of inhaled medicines and pollutants within alveoli. This will lead to a better understanding of aerosol mixing in these terminal air units. We aim to provide some insight from mathematics by modelling the motion of diffusing particles in alveolar flows, which is impossible to obtain through *in vivo* experiments. We shall now give some background about alveolar flow and the patterns that have been observed through numerical models and experimental studies.

Hundreds of millions of alveoli occupy a single adult lung [1]. The flow in these bulbous sacs is incompressible and Newtonian. The Reynolds number and the Womersley number are both much smaller than 1; this is based upon normal breathing frequencies [2]. Although air moves approximately like a Stokes flow, numerical and experimental observations have indicated that chaotic advection occurs in the alveoli [3–5].

For our purposes there are three key results, which have been found by Tsuda and his colleagues. Firstly, Tsuda *et al.* [4] constructed a numerical model of alveolar flow and determined that, for an alveolus of sufficient depth, recirculation can occur. Secondly, Tsuda *et al.* [5] created a series of flow visualization experiments on real alveoli and confirmed that, at the end of the first inhalation, a recirculation pattern forms. Thirdly, this pattern of recirculation can be disturbed on further ventilation, with good mixing of particles after three or four breathing cycles. These results suggest that chaotic advection can occur deep in the lung.

Recently, we have shown mathematically that an underlying pattern of recirculation can lead to chaotic particle trajectories [6]. This was achieved by focusing on two major features of alveolar flows, namely rotary motion and wall movement. A very simple mathematical model was built, based on the famous corner eddies of Moffatt [7]. Figure 1 shows sample trajectories depicting recirculation in a rigid corner; the flow is steady, so particle paths follow streamlines (see Acheson [8] for more details). This flow is perturbed by periodically expanding and contracting the walls. The results are remarkable: the effect of wall motion on recirculation generates regions in which particle transport is chaotic; elsewhere, the transport

*Department of Mathematics, University of Surrey, Guildford, GU2 7XH, UK. Email: f.laine-pearson@surrey.ac.uk p.hydon@surrey.ac.uk

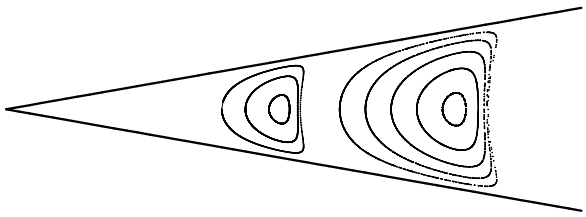

Figure 1: Moffatt's corner eddies with corner angle of 20°. Two eddies are shown; the left-hand eddy and the right-hand eddy are illustrated by three and five representative curves, respectively.

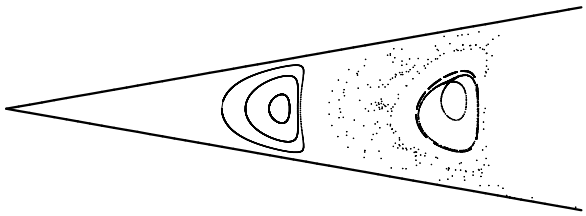

Figure 2: Moving the walls perturbs the eddies of Fig. 1. This Poincaré section shows that some of the eight representative curves have changed in structure.

is regular. Figure 2 gives an example of this structure; the illustration is a 'Poincaré section'; which is formed by plotting each particle's position as a point after every breathing cycle. More detailed figures are included in [6]. The structure can be explained by applying KAM (Kolmogorov-Arnol'd-Moser) theory and other associated theory from Hamiltonian dynamics [9, 10].

The experiments and the models that have been discussed so far have assumed that particles follow the alveolar flow. In reality, many inhaled particles do not do this. Some are small enough to diffuse; others are large enough to have substantial inertia. The current paper describes the transport of diffusing particles in the presence of recirculation. (By concentrating on these two features we will gain some understanding of how alveolar recirculation affects aerosol motion. We do not include wall motion, as diffusion renders KAM theory inapplicable.)

In §2 the flow field for the non-diffusing particle model [6, 7] is reviewed and the equations of motion are described as a Lagrangian system. The model is then adapted to accommodate diffusing particles, with the equations of motion expressed as a pair of coupled Langevin equations (these are Lagrangian equations of motion that have been adapted for stochastic particle motion). Results are given in §3.1 showing how recirculation can affect diffusing particles. In §3.2, a physical description of the model is used to explain our results. This leads to the discovery of the 'carousel effect', which allows diffusing particles to hop onto an eddy and, after a short time, hop off having been transported much further than could be achieved by diffusion alone. We also discuss the effects of varying parameters as well as explaining the physical mechanisms in the context of real alveoli. We summarize our conclusions in §4.

2 Method of Approach

We use carets to denote dimensional variables, which are removed when variables are non-dimensionalized.

2.1 Reviewing Non-diffusive Particle Motion

Moffatt formulated a model of Stokes flow of a fluid bounded by a corner whose walls are fixed with a unidirectional flow occurring far from the corner. He found that for angles of less than $2\phi_{\text{critical}} = 146.3°$, an infinite stream of eddies is produced in the corner [7]. Here we shall briefly review this model using the notation and formulation used in [6].

Let $\hat{\mathbf{u}} = \hat{u}_r \mathbf{e}_r + \hat{u}_\theta \mathbf{e}_\theta$ be the velocity field with respect to plane polar coordinates $(\hat{r}, \theta)$. As the corner region is simply-connected (that is, there are no holes in it) and the incompressibility condition is

$$\frac{1}{\hat{r}} \left(\hat{r}\hat{u}_r\right)_{,\hat{r}} + \frac{1}{\hat{r}} \left(\hat{u}_\theta\right)_{,\theta} = 0,$$

then there exists a streamfunction $\hat{\psi}(\hat{r}, \theta)$ such that $\hat{u}_r = \hat{\psi}_{,\theta}/\hat{r}$ and $\hat{u}_\theta = -\hat{\psi}_{,\hat{r}}$. Therefore we can describe particle motion by the equations

$$\frac{\mathrm{d}\hat{r}}{\mathrm{d}\hat{t}} = \frac{1}{\hat{r}}\hat{\psi}_{,\theta}, \quad \hat{r}\frac{\mathrm{d}\theta}{\mathrm{d}\hat{t}} = -\hat{\psi}_{,\hat{r}}.$$

The walls are at $\theta = \pm\phi_0$, where the parameter $2\phi_0$ is the corner angle. To guarantee recirculation it is presumed that $\phi_0 < \phi_{\text{critical}}$. The boundary conditions are

$$\hat{\psi}_{,\theta} = 0, \quad \hat{\psi}_{,\hat{r}} = 0 \quad \text{on} \quad \theta = \pm\phi_0.$$

Let a be the lengthscale for a particular eddy and let ψ_0 be the maximum value of $|\hat{\psi}|$ on that eddy. Then we nondimensionalize as follows:

$$\hat{\psi} = \psi_0 \psi, \quad \hat{r} = ar, \quad \hat{t} = \frac{a^2}{\psi_0} t.$$

The streamfunction is $\psi(r, \theta)$, which is explicitly written as

$$\psi = \mathrm{Re}\left\{K r^\lambda f(\theta, t)\right\}, \tag{1}$$

with

$$f = \cos((\lambda-2)\phi_0)\cos(\lambda\theta) - \cos(\lambda\phi_0)\cos((\lambda-2)\theta),$$

where the dominant eigenvalue λ, the complex amplitude K and the angle ϕ_0 are all scalars. Throughout this paper we shall choose $K = 1$ and $\phi_0 = 20°$.

The boundary conditions yield the eigenvalue equation

$$\sin(2\phi_0\mu) = -\mu\sin(2\phi_0), \quad \text{where} \quad \mu = \lambda - 1.$$

We consider only the flow corresponding to the dominant eigenvalues λ and $\bar{\lambda}$ (namely, the pair of eigenvalues with smallest positive real part). Moffatt showed that

$$\lambda = \left(1 + \frac{\xi}{2\phi_0}\right) + i\left(\frac{\eta}{2\phi_0}\right),$$

where $\xi \approx 4$ and η is $O(1)$.

In dimensionless variables, trajectories for particles that follow the flow are obtained from the Lagrangian equations of motion

$$\frac{\mathrm{d}r}{\mathrm{d}t} = \frac{1}{r}\frac{\partial\psi}{\partial\theta}, \quad \frac{\mathrm{d}\theta}{\mathrm{d}t} = -\frac{1}{r}\frac{\partial\psi}{\partial r}. \tag{2}$$

These equations adequately describe the motion of non-diffusing particles. We now show how the motion of diffusing particles can be modelled.

2.2 Modelling Diffusive Particle Motion

For diffusing particles there are additional terms added to the velocity field. In cartesian coordinates $\hat{x} = \hat{r}\cos\theta$, $\hat{y} = \hat{r}\sin\theta$, the particle motion is described by the Langevin equations

$$\frac{\mathrm{d}\hat{x}}{\mathrm{d}\hat{t}} = \hat{u}_x(\hat{x}(\hat{t}), \hat{y}(\hat{t})) + \hat{\chi}_1(\hat{t}), \tag{3}$$

$$\frac{\mathrm{d}\hat{y}}{\mathrm{d}\hat{t}} = \hat{u}_y(\hat{x}(\hat{t}), \hat{y}(\hat{t})) + \hat{\chi}_2(\hat{t}). \tag{4}$$

Here $\hat{\chi}_j$ are stochastic terms with zero mean and covariance $\langle\hat{\chi}_i(\hat{t})\hat{\chi}_j(\hat{t}+\hat{\tau})\rangle = 2D\delta_{ij}\delta(\hat{\tau})$, where D is the molecular diffusivity, δ_{ij} the Kronecker delta for $i, j = 1, 2$ and δ is the Dirac delta function; see Jones [11] for further details. The velocity components are

$$\hat{u}_x(\hat{x}(\hat{t}), \hat{y}(\hat{t})) = \hat{\psi}_{,\hat{y}} \quad \text{and} \quad \hat{u}_y(\hat{x}(\hat{t}), \hat{y}(\hat{t})) = -\hat{\psi}_{,\hat{x}},$$

where $\hat{\psi}$ is the Moffatt streamfunction written in cartesian coordinates. To nondimensionalize equations (3) and (4), use the scalings

$$\hat{x} = ax, \quad \hat{y} = ay, \quad \hat{\chi}_j = \sqrt{\frac{D\psi_0}{a^2}}\chi_j,$$

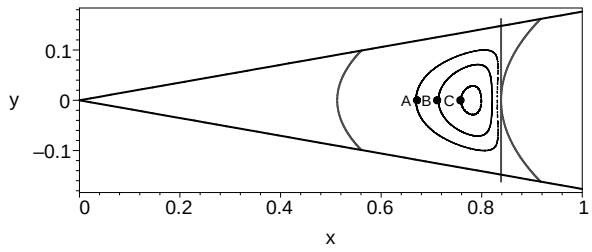

Figure 3: The inner three curves of the right-hand eddy of Fig. 1. The eddy is bound each side by a separatrix. The finish line is positioned at the minimum of the right-hand separatrix.

with the scaling for $\hat{\psi}$ and $\hat{t}$ introduced earlier. This transforms the Langevin equations (3) and (4) to their nondimensional form; in shorthand these are

$$\frac{\mathrm{d}x}{\mathrm{d}t} = \psi_{,y} + \frac{1}{\sqrt{\mathrm{Pe}}}\chi_1, \quad \frac{\mathrm{d}y}{\mathrm{d}t} = -\psi_{,x} + \frac{1}{\sqrt{\mathrm{Pe}}}\chi_2, \tag{5}$$

where $\mathrm{Pe} = \psi_0/D$ is a local (eddy-based) Péclet number.

In the results that follow we track particle paths by numerically integrating either equations (2) when $\mathrm{Pe} = 0$ or equations (5) when $\mathrm{Pe} \neq 0$ using a fourth-order Runge-Kutta method with a step size of 0.001 and incorporating a Maruyama adaption [12] for the contribution from diffusion; see [13, 14] for details.

3 Results

3.1 Recirculation Verses Diffusion

Figure 1 shows two eddies when $\mathrm{Pe} = 0$. We shall focus on the right-hand eddy. In particular, we use the set-up in Fig. 3. In between eddies there are separatrices; these have been numerically approximated in this figure. The initial positions for particle trajectories are $A = (0.670, 0)$, $B = (0.714, 0)$ and $C = (0.759, 0)$, which generate the three inner curves of the right-hand eddy of Fig. 1. For $\mathrm{Pe} \neq 0$, we release particle ensembles from points A, B and C. The ensembles are tracked and the first time that each particle crosses the finish line (held at $x = 0.839$, the x-value of the minimum of the right-hand separatrix) is recorded. Once a particle has crossed the finish line, it no longer participates. Figure 4 illustrates this for particles released from point A. The particles were tracked step-wise over a fixed maximum duration of time (10000 time steps). Figure 5 illustrates the crossing times for various Pe when particles are released from point A. We restricted our experiment

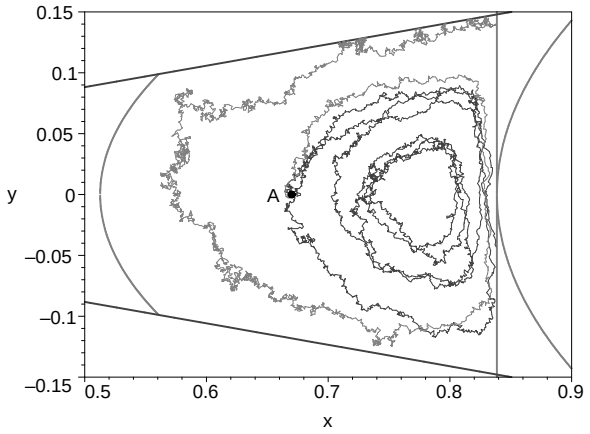

Figure 4: Two example trajectories of particles released from point A with Pe = 1000 (shown in black and grey respectively).

to Pe ≥ 1000 as these are typical values of physiological interest. Note that as Pe increases, diffusion decreases and the number of particles crossing the finish line decreases. Results for ensembles did not change significantly when the step size was halved. For an ensemble of N particles, the sample error is approximated as $1/\sqrt{N}$; see [12] for more details.

By fixing Pe = 10000 and tracking ensembles of 400 particles released from points A, B and C, we could gauge the importance of the release point. Figure 6 shows the crossing times for the particles. It is clear that starting further away from the centre of the right-hand eddy (but not too close to the walls) will encourage more particles to cross the finish line. Ensembles of 200 particles gave similar results, though the output was not as smooth. Figure 7 illustrates the crossing times when Pe = 1000. We will discuss these figures in more detail in §3.2.

The next part of the experiment compares the results found above with recirculation without diffusion and then for diffusion without recirculation. For recirculation alone, Fig. 8 illustrates how recirculation time decreases the closer into the eddy. For diffusion alone, Fig. 9 illustrates a two-dimensional random walk in a corner with two reflecting boundaries (at $\theta = \pm\phi_0$) and one absorbing boundary (the finish line). After 10000 time steps, none of the 200 particles released from A or B crossed the finish line; for point C, only 1.5% of particles passed the finish line. Decreasing Pe allows more particles to cross the finish line; see Fig. 10 for an illustration.

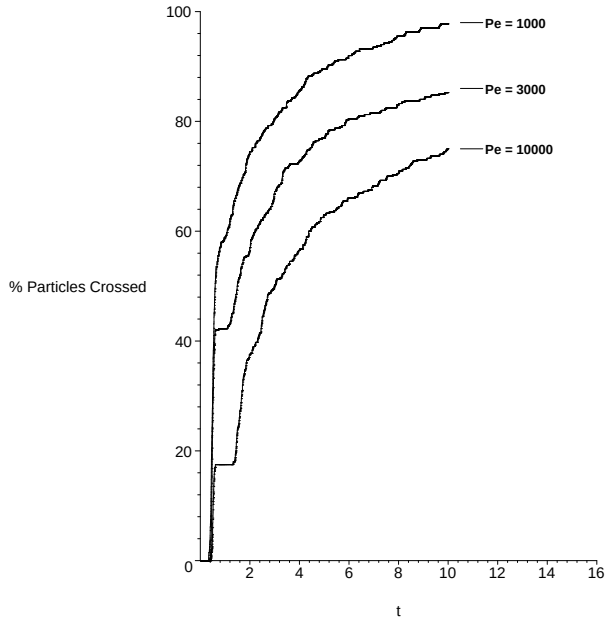

Figure 5: Crossing times for ensembles of 400 particles released from point A.

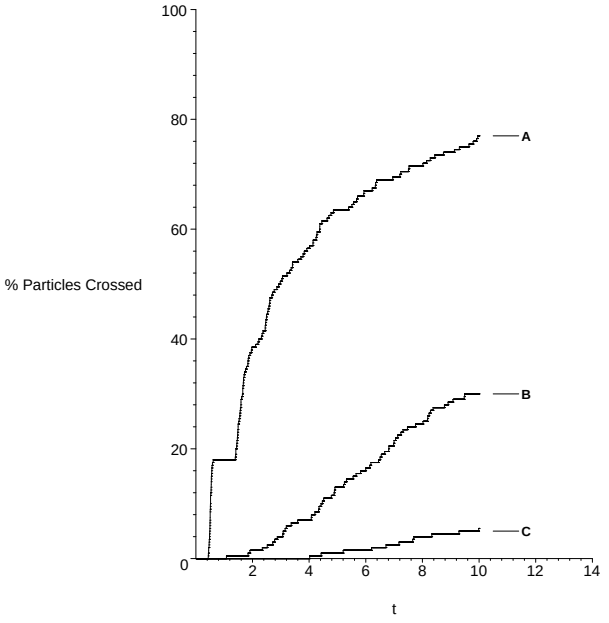

Figure 6: The crossing times for 400 particles released from points A, B and C, with Pe = 10000. Halving the ensemble size gave similar results.

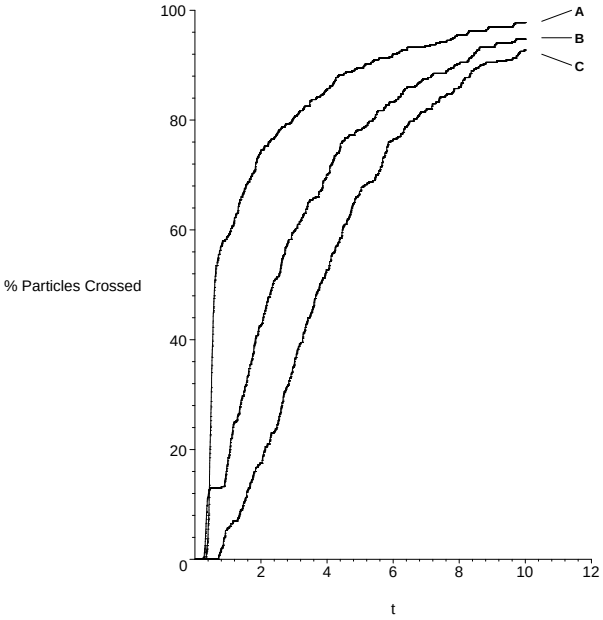

Figure 7: The crossing times for 400 particles released from points A, B and C, with Pe = 1000.

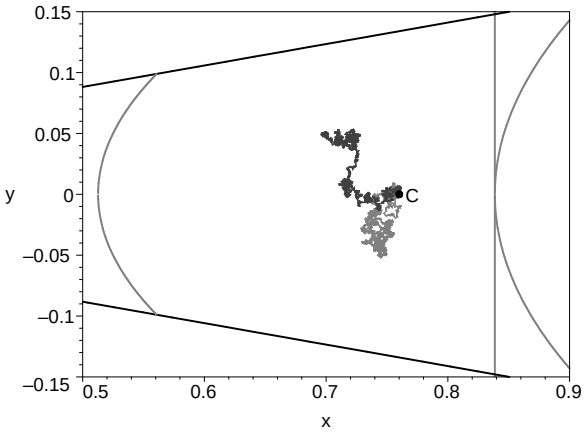

Figure 9: Two examples of two-dimensional random walk starting from point C with Pe = 10000 (shown in black and grey respectively).

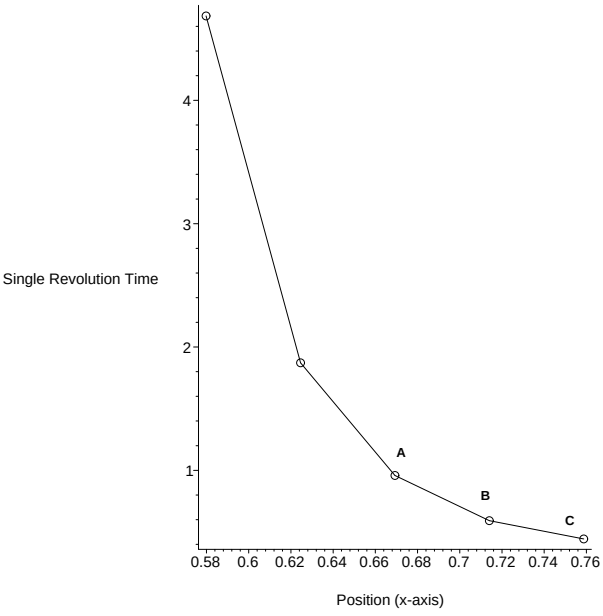

Figure 8: The time it takes for a particle released from $y = 0$ to complete a revolution when diffusion is not present.

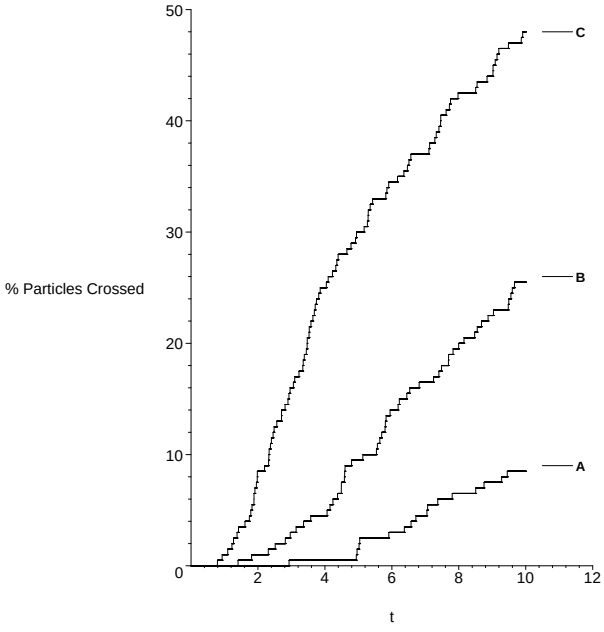

Figure 10: The crossing times for diffusion alone for 400 particles released from points A, B and C, with Pe = 1000.

By taking into account Figs 4, 6, 7, 9 and 10, it appears that introducing recirculation greatly enhances the transport of diffusing particles.

3.2 Discussion

Figures 6 and 7 will now be explained in more detail. Without diffusion (Fig. 1) particles released from points A, B and C cannot cross the finish line. However, adding diffusion creates the opportunity for particles to cross. With diffusion, it is clear that the further away a particle initially lies from the centre of the eddy, the quicker the ensemble will cross the finish line.

There is also a noticeable stepping occurring for the point A ensemble; see Fig. 6. (This was also observed for the other release points but the stepping is not as pronounced.) This stepping indicates that some of the particles diffuse out and cross the finish line during the first half-revolution, while the majority of particles are swept away by the recirculation and are forced to travel for approximately another revolution before some can pass the finish line; see also the single revolution times shown in Fig. 8 for time comparisons. After this initial settling, the particles then more regularly diffuse over the finish line. The effect is not so exaggerated for points B and C — this pair of ensembles takes a much longer time to spiral out to the finish line as they have essentially more ground to cover.

Figure 11 shows a log plot of the number of particles that do not cross the finish line; it corresponds with Fig. 7. The long-term transport behaviour shown in this plot indicates exponential decay $\exp(-kt)$, where k is the long-term decay rate. The decay rate for particles released from points A, B and C of Fig. 11 is $k \approx 0.3$. Without recirculation (Fig. 12), the decay rate is $k \approx 0.01, 0.04, 0.06$, for points A, B and C respectively. Therefore, it is clear that the recirculation greatly enhances transport of diffusing particles. This enhanced transport mechanism, which we call the 'carousel effect', encourages particles to diffuse into a recirculation zone for a short time, leaving the zone having been transported much further than is possible by diffusion alone. Figure 13 illustrates this mechanism and Fig. 7 is another example of this mechanism in practice.

From [6] it is known that when only recirculation is present, particles travelling on eddies that lie closer to the apex of the corner move more slowly than those on eddies lying far away. For instance, the left-hand

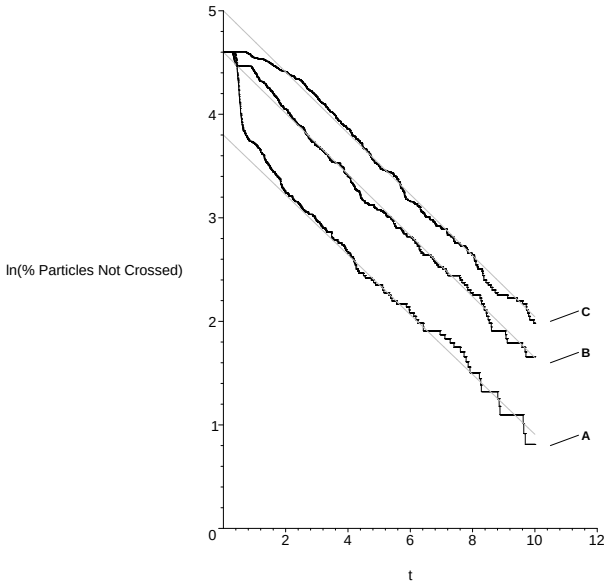

Figure 11: The percentage of particles with recirculation present and remaining to the left of the finish line. These were released from points A, B and C, with Pe = 1000. (Lines of best fit are shown in grey.)

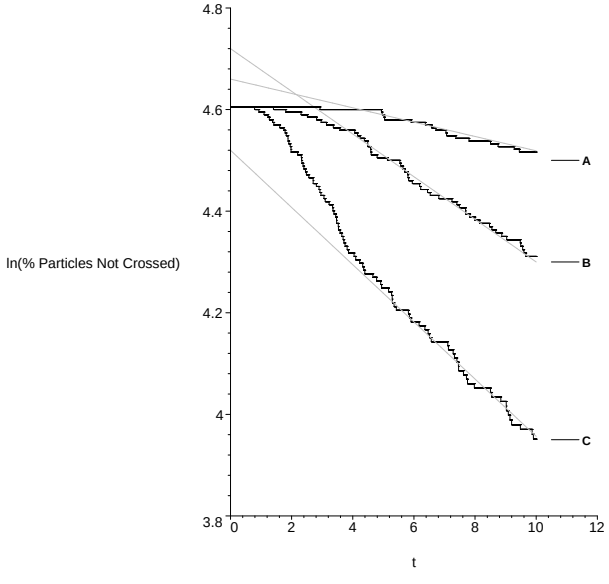

Figure 12: The percentage of particles that remain to the left of the finish line. These were released from points A, B and C, with the same diffusivity as in Fig 11 but without recirculation. (Lines of best fit are shown in grey.)

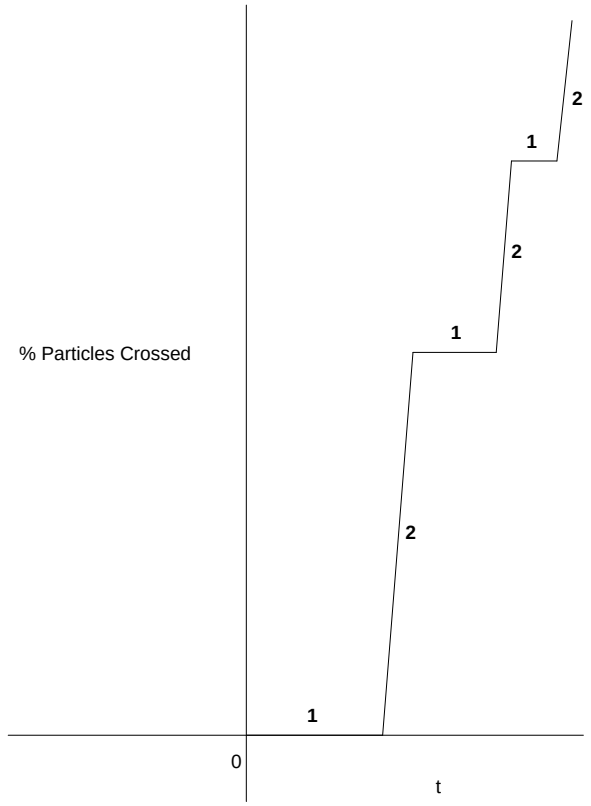

Figure 13: Step 1: Particle goes around on eddy (carousel). Step 2: Many particles diffuse off the eddy and cross the finish line.

eddy in the 20° corner is around 380 times weaker than the right-hand eddy. Hence particle paths in the left-hand eddy will resemble those in the absence of recirculation.

In the context of real alveoli, our results imply that an underlying pattern of recirculation could, if sufficiently strong enough, enhance the transport of diffusing particles. This, in turn, would enhance mixing. Although our model is very simple, it does indicate that the effect of diffusion in a recirculatory flow can make a considerable difference to whether a particle is retained in the alveolus or not.

From a qualitative viewpoint, increasing the angle of the corner (up to the critical angle) will do two things to the relative recirculations of eddy sequences: it will increase the relative sizes and increase the relative strengths [7]. However, as the Péclet number is eddy-based, neighbouring eddies will feel the effect of diffusion in a scaled sense. (For an arbitrary fixed corner angle in the eddy-generating regime, the right-hand eddy will be, say, X times stronger than its left-hand neighbour and this is reflected in ψ_0. So by fixing D, the Péclet number of the right-hand eddy will be larger than that of its left-hand neighbour by about a factor of X.) Increasing the value of K will increase the speed of particles. By exchanging constant K with $K(t)$, it is possible to make the flow past the corner alternating, which would then incorporate a periodic bidirectional flow. By doing so, the impact of diffusion would be altered. Another factor to consider would be the effect of wall motion. For the corner model, diffusion with very large Pe would blur the structures depicted in the Poincaré section of Fig. 2. As Pe decreases, diffusion completely hides the structures.

4 Conclusions

We have identified an enhanced transport mechanism, called the carousel effect. For sufficiently strong recirculation, particles are able to diffuse into a recirculation zone for some time and then to leave it having being transported much further than is possible by diffusion alone. This mechanism may play an important part in mixing and retention of aerosols deep in the lung.

Acknowledgements

F. E. L.-P. and P. E. H. are supported by the NIH under grant number BRP HL070542. This is a col-

laborative project led by Akira Tsuda of the Harvard School of Public Health.

References

[1] Ochs, M., Nyengaard, J. R., Jung, A., Knudsen, L., Voigt, M., Wahlers, T., Richter, J., and Gundersen, H. J. G., 2004, "The Number of Alveoli in the Human Lung," Am. J. Respir. Crit. Care. Med., 169, pp. 120-124.

[2] Haber, S., Butler, J. P., Brenner, H., Emanuel, I., and Tsuda, A., 2000, "Shear Flow over a Self-similar Expanding Pulmonary Alveolus during Rhymical Breathing," J. Fluid Mech., 405, pp. 243-268.

[3] Tippe, A., and Tsuda, A., 1999, "Recirculating Flow in an Expanding Alveolar Model: Experimental Evidence of Flow-induced Mixing of Aerosols in the Pulmonary Acinus," J. Aerosol Sci., 31(8), pp. 979-986.

[4] Tsuda, A., Henry, F. S., and Butler, J. P., 1995, "Chaotic Mixing of Alveolated Duct Flow in Rhythmically Expanding Pulmonary Acinus," J. Appl. Physiol., 79, pp. 1055-1063.

[5] Tsuda, A., Rogers, R. A., Hydon, P. E., and Butler, J. P., 2002, "Chaotic Mixing Deep in the Lung," Proc. Nat. Acad. Sci., 19, pp. 10173-10178.

[6] Laine-Pearson., F. E., and Hydon, P. E., 2006, "Particle Transport in a Moving Corner," J. Fluid Mech., 559, pp. 379-390.

[7] Moffatt, H. K., 1964, "Viscous and Resistive Eddies near a Sharp Corner," J. Fluid Mech., 18, pp. 1-18.

[8] Acheson, D. J., 1990, Elementary, Fluid Dynamics, Oxford University Press, Oxford, UK, Chap. 1.

[9] Lichtenberg, A. J., and Lieberman, M. A., 1992, Regular and Chaotic Dynamics, Springer-Verlag, Berlin, Germany.

[10] Tabor, M., 1989, Chaos and Integrability in Nonlinear Dynamics, Wiley, USA.

[11] Jones, S. W., 1994, "Interaction of Chaotic Advection and Diffusion," Chaos, Solitons & Fractals, 4(6), pp. 929-940.

[12] Higham, D. J., 2001, "An Algorithmic Introduction to Numerical Simulation of Stochastic Differential Equations," SIAM Review, 43(3), pp. 525-546.

[13] Diamantopoulos, A., and Schlegelmilch, B. B., 2000, Taking the Fear Out of Data Analysis, Thomson Learning, London, UK.

[14] Press, W. H., Flannery, B. P., Teukolsky, S. A. and Vetterling, W. T., 1992, Numerical Recipes in C: The Art of Scientific Computing, 2nd Ed., Cambridge University Press, Cambridge, UK.

Figure Captions — For Production Purposes Only

Figure 1: Moffatt's corner eddies with corner angle of 20°. Two eddies are shown; the left-hand eddy and the right-hand eddy are illustrated by three and five representative curves, respectively.

Figure 2: Moving the walls perturbs the eddies of Fig. 1. This Poincaré section shows that some of the eight representative curves have changed in structure.

Figure 3: The inner three curves of the right-hand eddy of Fig. 1. The eddy is bound each side by a separatrix. The finish line is positioned at the minimum of the right-hand separatrix.

Figure 4: Two example trajectories of particles released from point A with Pe = 1000 (shown in black and grey respectively).

Figure 5: Crossing times for ensembles of 400 particles released from point A.

Figure 6: The crossing times for 400 particles released from points A, B and C, with Pe = 10000. Halving the ensemble size gave similar results.

Figure 7: The crossing times for 400 particles released from points A, B and C, with Pe = 1000.

Figure 8: The time it takes for a particle released from $y = 0$ to complete a revolution when diffusion is not present.

Figure 9: Two examples of two-dimensional random walk starting from point C with Pe = 10000 (shown in black and grey respectively).

Figure 10: The crossing times for diffusion alone for 400 particles released from points A, B and C, with Pe = 1000.

Figure 11: The percentage of particles with recirculation present and remaining to the left of the finish line. These were released from points A, B and C, with Pe = 1000. (Lines of best fit are shown in grey.)

Figure 12: The percentage of particles that remain to the left of the finish line. These were released from points A, B and C, with the same diffusivity as in Fig 11 but without recirculation. (Lines of best fit are shown in grey.)

Figure 13: Step 1: Particle goes around on eddy (carousel). Step 2: Many particles diffuse off the eddy and cross the finish line.